ADVANCED ENGINEERING MATERIALS
www.aem-journal.com

Exploiting Geometric Frustration in Coupled von Mises Trusses to Program Multifunctional Mechanical Metamaterials

*Yannis Liétard, Daniel Therriault, and David Melancon**

Multistable mechanical metamaterials are an emerging class of materials whose intricate internal structure can be engineered to program mechanical properties and promote reversible transitions between multiple stable states of energy. In this work, the design of a mechanical metamaterial based on an assembly of bistable von Mises trusses is presented. It is shown that coupling two von Mises trusses induces geometric frustration, which leads to an asymmetry between the stable states. Then the von Mises trusses are combined to build a unit cell that can change effective stiffness in compression when switching states. Based on a semi-analytical model, the stiffness variation is characterized as a function of the geometric parameters and three possible scenarios are highlighted: 1) increased, 2) decreased, or 3) constant stiffness between the stable states. To validate the concept, the multistable metamaterials out of polylactic acid and thermoplastic polyurethane via fused filament fabrication are fabricated, and their mechanical response is evaluated by measuring experimentally the effective stiffness in both stable states under compression. This unit cell also features modularity, enabling reversible assembly and post-fabrication tunability. Finally, a range of applications are explored, including sandwich panels capable of changing their compressive and bending stiffness as well as their surface morphology.

1. Introduction

Recent advances in the field of mechanical metamaterials have significantly enhanced the tunability of their mechanical properties.[1–3] Among these, stiffness stands out as a particularly important attribute. The manipulation of stiffness has been successfully achieved through various innovative mechanisms, such as origami- and kirigami-inspired designs,[4–12] topological transformations,[13,14] and stimuli-responsive materials.[15–17] The capability to tune material stiffness opens up a multitude of applications, including soft grippers,[5,18] smart fabrics,[19] structures that soften to prevent damage during collisions,[20] sensing and data transmission,[21,22] as well as biomimetic robots.[23] Another exotic property of mechanical metamaterials is shape morphing, which allows them to be reconfigured and undergo significant and reversible changes in shape.[4,24–27] Some mechanical metamaterials utilize mechanisms to retain specific shapes without the need for constant actuation.[13,28–33] These shape-morphing capabilities are particularly useful for applications such as aerodynamic drag control,[34] morphing drones and underwater machine,[27] or deployable implants for minimally invasive surgery.[35] Moreover, recent research has underscored the importance of modularity, which enables mechanical properties to be tuned post-fabrication,[36–39] enhancing the versatility and adaptability of mechanical metamaterials.

While these three properties—tunable stiffness, shape morphing, and modularity—have been mostly developed separately, here, we propose a multistable mechanical metamaterial that combines them all. To achieve this purpose, we first take inspiration from a simple bistable building block shown in **Figure 1**A: the von Mises truss. By coupling two independent von Mises trusses, we show that this can lead to two stable states with distinct energy levels separated by ΔU (Figure 1B). This is the starting point of a bottom-up strategy to program the mechanical behavior of multistable unit cells combining four coupled von Mises trusses described in Figure 1C. Our unit cell displays tunable compressive stiffness in its different stable states (Figure 1D), post-fabrication reconfigurability through modularity (Figure 1E), and shape-morphing capabilities (Figure 1F). We subsequently utilize these properties to create sandwich panels

Y. Liétard, D. Therriault, D. Melancon
Laboratory for Multiscale Mechanics
Department of Mechanical Engineering
Polytechnique Montréal
2500 Chemin de Polytechnique, Montréal, Québec H3T 1J4, Canada
E-mail: david.melancon@polymtl.ca

Y. Liétard, D. Therriault, D. Melancon
Research Center for High Performance Polymer and Composite Systems (CREPEC)
Department of Mechanical Engineering
McGill University
817 rue Sherbrooke Ouest, Montréal, Québec H3A 0C3, Canada

The ORCID identification number(s) for the author(s) of this article can be found under https://doi.org/10.1002/adem.202402006.

DOI: 10.1002/adem.202402006

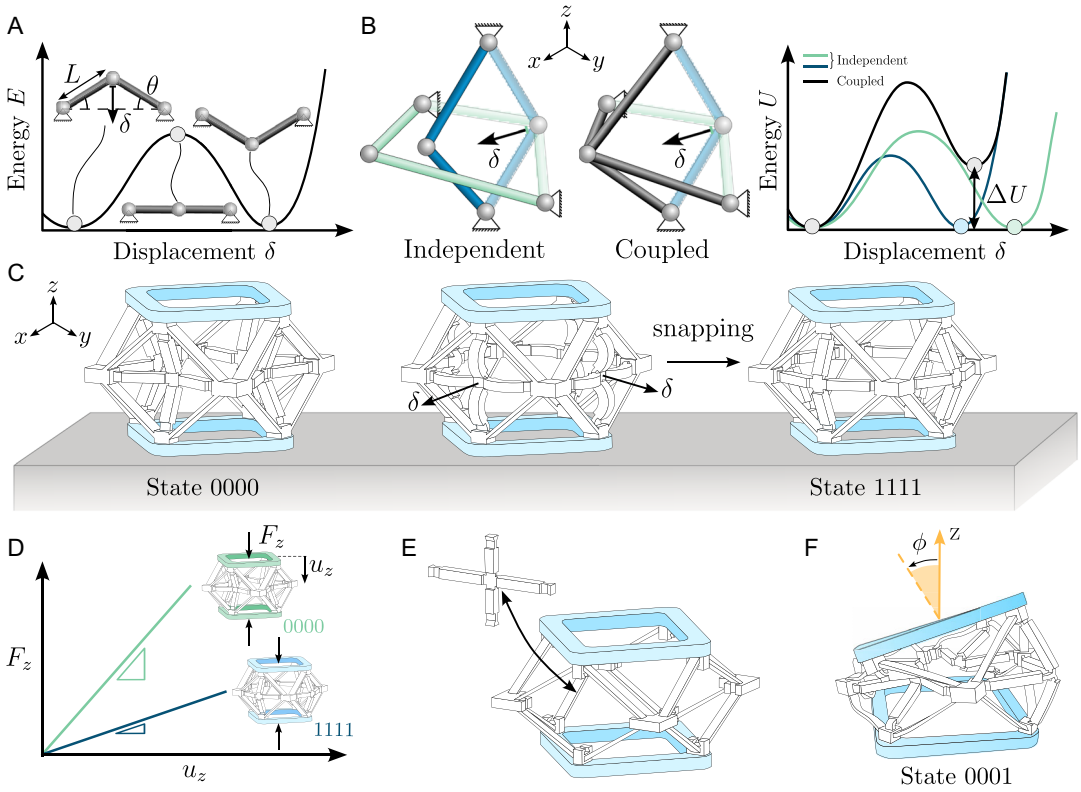

Figure 1. Multistable mechanical metamaterials capable of stiffness tunability, modularity, and shape morphing. A) A bistable von Mises truss can be characterized by an initial length L and an initial angle θ. The energy landscape of this bistable structure exhibits two energy wells with equivalent strain energy levels. B) When coupled, two von Mises trusses with non-coplanar extremities form a building block with nonzero energy in the second stable state, as evidenced by ΔU. C) Four building blocks are assembled to form a unit cell. Each building block corresponds to a face of the unit and has two stable states, 0 and 1. When all the faces are in the first stable state, the unit is in state 0000, and when all the faces are in the second stable state, the unit is in state 1111. D) Our unit cell is capable of changing stiffness in compression when switching from state 0000 to state 1111. E) The fabrication process of the unit enables reversible assembly of the von Mises trusses, making it possible to easily change the unit's properties post-fabrication. F) When activating only one face in state 0001, the height of this side changes, causing the unit to bend and offering potential for shape-morphing applications. Note that each unit's drawing is adapted from an image taken from a 3D-printed prototype.

with adjustable compressive and bending stiffness, as well as morphing surfaces.

2. Results

2.1. Coupled von Mises Trusses Exhibiting Geometric Frustration

Our bistable building block draws inspiration from the von Mises truss, a well-recognized concept employed to achieve bistability,[14,28,40] comprising an assembly of two trusses pinned at their apex and simply supported at their lower ends. A von Mises truss can be characterized by two geometric parameters: θ, representing the initial angle of inclination of the two trusses relative to the horizontal plane, and L, denoting the initial length of one truss. When a displacement δ is applied at its apex, the von Mises truss undergoes a deformation that is characterized by an energy landscape with stable states of identical strain energy level (see Figure 1A). We obtain a similar behavior for all von Mises trusses characterized by $L > 0$ and $\theta \in [0°, 90°]$. To achieve a broader range of responses, we propose a building block which consists in an assembly of two coupled von Mises trusses. These coupled von Mises trusses can be characterized by three geometric parameters forming our design space: 1) θ_{0xy} and 2) θ_{0xz}, representing the initial angles of the von Mises trusses in the xy plane and xz plane, respectively, and 3) $r_L = L_{0xy}/L_{0xz}$, the ratio of the initial lengths (see **Figure 2**A). Another important geometrical characteristic is the distance Δ, defined as the algebraic distance between a first line connecting the two ends of the von Mises truss in the xz plane and a second line connecting the ends of the von Mises truss in the xy plane:

$$\Delta = L_{0xz}\left(\sin\theta 0_{xy} - r_L \sin\theta_{xy}\right) \tag{1}$$

We first characterize the energy landscape of our coupled von Mises trusses by conducting Finite-element (FE) simulations (ABAQUS 2022). Exploiting symmetry, we model one quarter of the structure using beam elements. To account for potential large deformation, we use an incompressible neo–Hookean hyperelastic model with initial Young's modulus E_0 (in ABAQUS 2022 the input parameters are $C10 = E_0/6$ and $D1 = 0$—see Section S2, Supporting Information, for details).

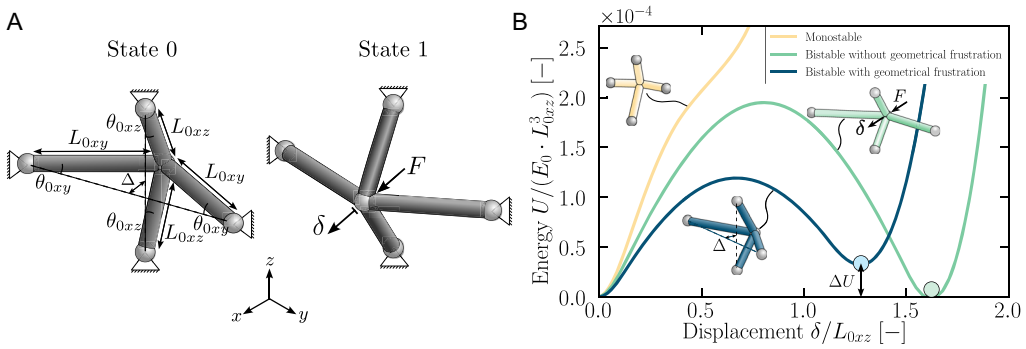

Figure 2. Building block based on coupled von Mises trusses. A) The building block can be characterized by three design parameters: the ratio of the initial length $r_L = L_{0xy}/L_{0xz}$ and two initial angles θ_{0xy} and θ_{0xz}. The initial state is denoted as state 0, while the second stable state is referred to as state 1. B) The building block is initially analyzed using a finite-element model to characterize the evolution of the normalized elastic energy, $U/(E_0 \cdot L_{0xz}^3)$ as a function of the normalized displacement, δ/L_{0xz} applied at the central vertex. We find three distinct scenarios: monostable (yellow curve), bistable without geometric frustration (green curve), when all four extremities are coplanar, and bistable with geometric frustration (blue curve), when the four extremities are not coplanar. Non-coplanar geometries are characterized by the distance Δ, which is defined as the algebraic distance between a first line connecting the two ends of the von Mises truss in the *xz* plane and a second line connecting the ends of the von Mises truss in the *xy* plane.

When a displacement δ is imposed on the central node, three distinct scenarios can emerge. First, if the four simply supported nodes lie on the same plane, i.e., for double von Mises trusses characterized by $\Delta/L_{0xz} = 0$, there is no geometric frustration in the second stable state and the two local minima have the same energy level (see green curve in Figure 2B). Instead, if the four extremities are not coplanar, i.e., for double von Mises trusses characterized by $\Delta/L_{0xz} \neq 0$, geometric frustration arises in the second stable state because both von Mises trusses cannot simultaneously minimize their energy (see the blue curve in Figure 2B). Finally, if geometric frustration is too high, the double von Mises truss becomes monostable (see the yellow curve in Figure 2B). The asymmetry induced by geometric frustration between the two stable states can potentially result in distinct mechanical properties. This finding, along with recent research leveraging geometric frustration to design programmable metamaterials,[2,12] motivated us to utilize the proposed building block in the construction of a mechanical metamaterial unit.

2.2. Unit Cell with Tunable Mechanical Properties

Having demonstrated that coupled von Mises trusses can display geometric frustration in its second stable state, we use it to form a mechanical metamaterial unit cell capable of tuning compressive stiffness (see **Figure 3**A where each of the four faces of the unit cell corresponds to coupled von Mises trusses). Depending on the state of the unit's faces, i.e., 0000, indicating that all four faces are folded inward, and 1111, indicating that they are snapped outward, the compressive stiffness may vary. We begin by conducting FE analyses using ABAQUS 2022 to predict the mechanical response in compression of our unit. Taking advantage of the symmetry of the structure, we model a quarter of a unit's face of dimension $L_{0xz} = 10$ mm using an unstructured mesh of 8-node linear volumetric elements and an incompressible neo–Hookean hyperelastic model with initial Young's modulus $E_0 = 28$ MPa (see details of the FE simulation in Section S2, Supporting Information). The stiffness variation, η, is calculated as the ratio of the stiffness in state 1111, K_{1111}, over the stiffness in state 0000, K_{0000}. As revealed by our simulations on the coupled von Mises trusses, we expect negligible change in compressive stiffness between states 0000 and 1111 for a geometry where the four extremities lie on the same plane, i.e., $\Delta = 0$ mm. We simulate the response of an iso-stiffness unit with ($r_L^{\text{iso}} = 2.0$, $\theta_{0xy}^{\text{iso}} = 21°$, $\theta_{0xz}^{\text{iso}} = 40°$) and find similar effective compressive stiffness of $(K_{0000}^{\text{iso}})_{\text{FE}} = 10.1\ \text{N mm}^{-1}$ and $(K_{1111}^{\text{iso}})_{\text{FE}} = 11.6\ \text{N mm}^{-1}$, in both stable states (see green bars in Figure 3B), resulting in a stiffness variation of $\eta_{\text{FE}}^{\text{iso}} = 1.15$. This discrepancy from the expected stiffness variation of 1 could be coming from the fact that while assembling the initially flat coupled von Mises trusses into the frame, we induce a small elastic deformation that is located in the joints (see Section S2, Supporting Information, for details). Instead, if the four extremities are not coplanar, i.e., $\Delta \neq 0$ mm, geometric frustration in the second stable state will induce a change in compressive stiffness. We consider two additional geometries for which 1) Δ is negative, i.e., $\Delta^{\text{soft}} = -3.22$ mm with ($r_L^{\text{soft}} = 2.0$, $\theta_{0xy}^{\text{soft}} = 25°$, $\theta_{0xz}^{\text{soft}} = 30°$) and 2) Δ is positive, i.e., $\Delta^{\text{stiff}} = 2.78$ mm with ($r_L^{\text{stiff}} = 2.0$, $\theta_{0xy}^{\text{stiff}} = 20°$, $\theta_{0xz}^{\text{stiff}} = 55°$). Note that these values of Δ can be extracted from Equation (1) by adding 3 mm to the length of L_{0xz} to account for the 3D-printed joints (see Figure S1, Supporting Information, for details.) For the first non-coplanar unit, our FE simulations predict a softening behavior, with values of the effective compressive stiffness dropping from $(K_{0000}^{\text{soft}})_{\text{FE}} = 14.2\ \text{N mm}^{-1}$ to $(K_{1111}^{\text{soft}})_{\text{FE}} = 2.18\ \text{N mm}^{-1}$ (see blue bars in Figure 3B), yielding a stiffness variation of $\eta_{\text{FE}}^{\text{soft}} = 0.15$. In contrast, for the second non-coplanar unit, we find a stiffening behavior with $(K_{0000}^{\text{stiff}})_{\text{FE}} = 4.89\ \text{N mm}^{-1}$ to $(K_{1111}^{\text{stiff}})_{\text{FE}} = 20.6\ \text{N mm}^{-1}$ (see red bars in Figure 3B), which leads to a stiffness variation of $\eta_{\text{FE}}^{\text{stiff}} = 4.2$.

To experimentally investigate the compressive stiffness variation of the unit when switching from state 0000 (Figure 3A(i)) to state 1111 (Figure 3A(ii)), we fabricate the iso-stiffness,

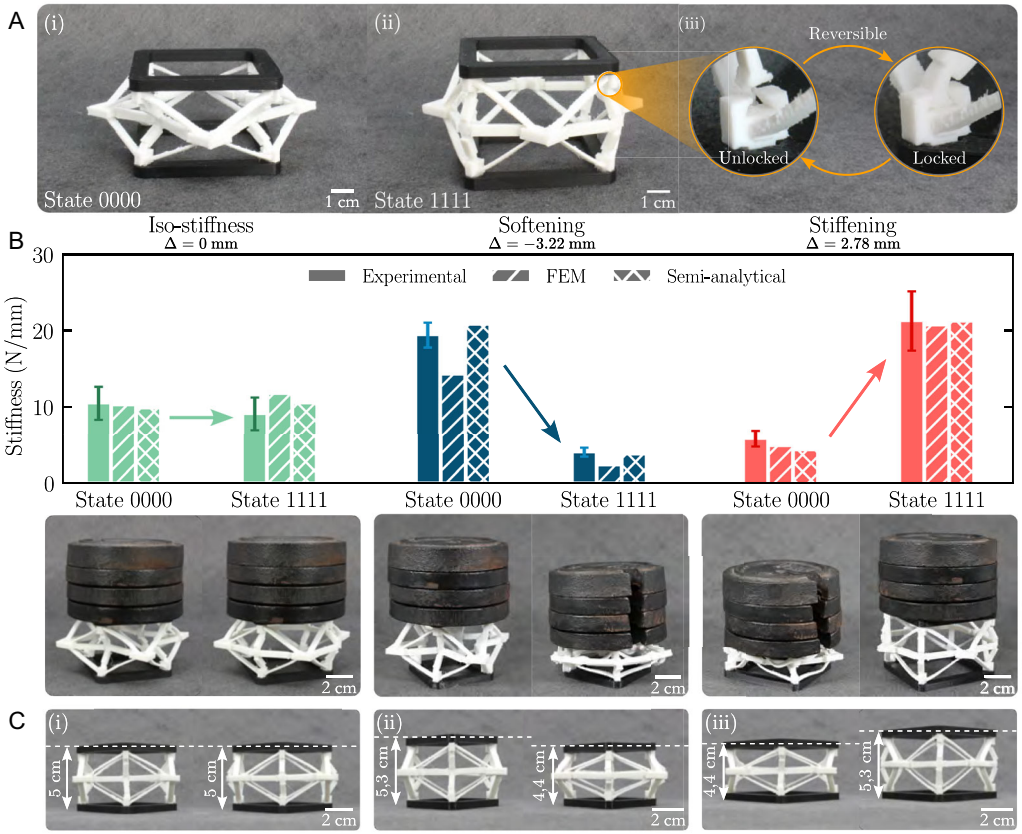

Figure 3. Tunable mechanical properties. A) A mechanical metamaterial unit cell consisting of an assembly of four building blocks. i) When all four faces are in their initial state, this configuration is denoted as state 0000. ii) Conversely, when all faces are in the second stable state, this configuration is referred to as state 1111. iii) The coupled von Mises trusses are assembled with an interlocking mechanism that allows for reversible assembly, thereby making the unit modular. B) Three different designs are experimentally tested in compression: an iso-stiffness unit, with no stiffness variation between the two stable states; a softening unit, showcasing decreasing stiffness; and a stiffening unit, demonstrating increasing stiffness. Experimental uncertainties were obtained by repeating the tests on three samples, five times for each sample. C) i) The iso-stiffness unit does not change height when switching from state 0000 to state 1111, ii) the softening unit exhibits decreasing height, and iii) the stiffening unit demonstrates increasing height.

softening, and stiffening units out of thermoplastic polyurethane (white thermoplastic polyurethane (TPU) from Polymaker with $E_0 = 28$ MPa). Note that we add rigid parts on the top and bottom of the unit to ensure smooth load transfer during mechanical tests (black PLA from Ultimaker). Additional details on the fabrication process can be found in Section S1, Supporting Information. A sliding mechanism is used to fix the coupled von Mises trusses to the frame, as presented in Figure 3A(iii), which enables reversible assembly to modify the unit's properties after manufacture. Note that this assembly induces a small initial deformation in the unit's joints which is captured by our FE model (see Section S2, Supporting Information, for details). Compression tests are performed (MTS Insight electromechanical machine, MTS Systems Corporation, Eden Prairie, Minnesota, US) with a displacement-controlled load (10 mm min^{-1}) in states 0000 and 1111 to evaluate the effective stiffness in compression, which is given by the slope of the force–displacement curve in the linear regime (see Figure 3B). For the iso-stiffness unit, the stiffness values in states 0000 and 1111 are $(K^{\text{iso}}_{0000})_{\text{exp}} = 10.4 \pm 2.15$ N mm^{-1} and $(K^{\text{iso}}_{1111})_{\text{exp}} = 9.01 \pm 2.13$ N mm^{-1}, respectively (see green bars in Figure 3B), resulting in a stiffness variation of $\eta^{\text{iso}}_{\text{exp}} = 0.87$. This minimal stiffness variation is demonstrated visually by placing a weight of 1.7 kg on top of the unit in both stable states in Figure 3B, where no change is observed in the deformation. The experimental results for the softening unit reveal a stiffness of $(K^{\text{soft}}_{0000})_{\text{exp}} = 19.3 \pm 1.62$ N mm^{-1} in state 0000 and $(K^{\text{soft}}_{1111})_{\text{exp}} = 3.88 \pm 0.571$ N mm^{-1} in state 1111. Compressive stiffness decreases when all faces are actuated, as evidenced by a stiffness variation of $\eta^{\text{soft}}_{\text{exp}} = 0.20$. While the unit in the first stable can withstand a weight of 1.7 kg, it fails under the same load in the second stable state (see insets in Figure 3B). Lastly, for the stiffening unit, we measure a stiffness of $(K^{\text{stiff}}_{0000})_{\text{exp}} = 5.82 \pm 1.01$ N mm^{-1} in state 0000 and $(K^{\text{stiff}}_{1111})_{\text{exp}} = 21.2 \pm 3.86$ N mm^{-1} in state 1111. The resulting stiffness variation is $\eta^{\text{stiff}}_{\text{exp}} = 3.64$, confirming that stiffness can increase as well. Whereas the unit yields under a load of 1.7 kg in the first stable state, it can support the same load in the second stable state (see insets in Figure 3B). Overall, for the three geometries studied, the experimental results are in good agreement with the FE simulations.

In addition to the ability to modify stiffness, the proposed unit cell also demonstrates shape-morphing abilities. As illustrated in Figure 3C, the height of a unit can be altered through the actuation of its faces. Similar to the results observed for stiffness variation, three distinct behaviors are identified. For the iso-stiffness unit, no height variation is detected. Conversely, for the softening unit, the height decreases from 5.3 to 4.4 cm when transitioning from the first stable state to the second. Finally, for the stiffening unit, the height increases from 4.4 to 5.3 cm.

Motivated by the ability to tune stiffness and height, we develop a semi-analytical model to map the stiffness and height variation of the unit across our design space and to gain more insight into the underlying causes of these variations. Our model is based on a combination of axial and torsion springs, to represent the trusses and the joints, respectively, along with Euler–Bernoulli beams to model the beams of the frames. The energy of the system in both stable states under compression can be determined by using the principle of minimum potential energy. The corresponding force–displacement curves are then derived by differentiating the energy with respect to displacement. The stiffness in each stable state is calculated as the initial slope of the force–displacement curves (see details on the semi-analytical model in Section S3, Supporting Information). This approach enables rapid evaluation of stiffness and height variation. The semi-analytical model's predictions for the stiffness values of the iso-stiffness unit ($(K^{\text{iso}}_{0000})_{\text{sa}} = 9.74\,\text{N mm}^{-1}$, $(K^{\text{iso}}_{1111})_{\text{sa}} = 10.4\,\text{N mm}^{-1}$), the softening unit ($(K^{\text{soft}}_{0000})_{\text{sa}} = 20.7\,\text{N mm}^{-1}$, $(K^{\text{soft}}_{1111})_{\text{sa}} = 3.59\,\text{N mm}^{-1}$), and the stiffening unit ($(K^{\text{stiff}}_{0000})_{\text{sa}} = 4.32\,\text{N mm}^{-1}$, $(K^{\text{stiff}}_{1111})_{\text{sa}} = 21.1\,\text{N mm}^{-1}$) closely align with the experimental results, therefore validating the model (see Figure 3B).

We use our semi-analytical model to conduct a parametric study over a design space characterized by $[r_L, \theta_{0xy}, \theta_{0xz}] \in [0.5, 2.0] \times [10°, 70°] \times [10°, 70°]$. For each variable, we use 10 linearly spaced points, leading to 1000 different geometries. The parametric study reveals various possible scenarios: 1) monostable, 2) no stiffness variation, 3) decreased stiffness, and 4) increased stiffness and height. In particular, **Figure 4** shows the influence of the geometrical parameter Δ on the stiffness ratio η (see Figure S10, Supporting Information, for the influence on height variation). When $\Delta = 0$, the four extremities of the von Mises trusses are coplanar and no stiffness variation is observed. Then, two different behaviors are observed depending on the sign of Δ. With the exception of a few cases, when Δ is negative, the stiffness of the unit decreases when switching from state 0000 to state 1111. In contrast, when Δ is positive, the stiffness increases. The influence of Δ can be explained by the fact that the stiffness of the unit essentially comes from the von Mises trusses in the *xz* plane, highlighted in blue and red in the insets of Figure 4. When these trusses are completely vertical (i.e., $\theta_{0xz} = 0°$), they are solicited purely axially, making the unit very stiff. In contrast, when the trusses are inclined (i.e., θ_{0xz} is maximal), resistance is mainly provided by the joints and the unit is very soft. When $\Delta < 0$, the initial angle in the first stable state, θ_{0xz}, is smaller than the angle in the second stable state, θ_{1xz}, (see the highlighted blue trusses in Figure 4) which is why the stiffness decreases. Conversely, when $\Delta > 0$, θ_{0xz} is bigger than θ_{1xz} (see the highlighted red trusses in Figure 4), resulting in an increased stiffness. The bounds of the stiffness variation can be determined by considering limit cases. The softest configurations are obtained when the value of θ_{0xz} is maximal. By only considering the stiffness of the joints, we can calculate a lower limit of the unit's stiffness $K_{\min} = 1.4\,\text{N mm}^{-1}$. The stiffest configurations are obtained when $\theta_{0xz} = 0°$. By only considering the axial stiffness of the vertical von Mises trusses, we find an upper limit $K_{\max} = 88\,\text{N mm}^{-1}$ (the derivation of $K_{\min}$ and $K_{\max}$ can be found in Section S3, Supporting Information). Therefore, the stiffness variation is expected to lie within an interval $[K_{\min}/K_{\max}, K_{\max}/K_{\min}] = [0.016, 63]$, which is in good agreement with the results given by the semi-analytical model, confirming the predominant role of the initial inclination of the von Mises trusses in the *xz* plane on the compressive stiffness of the unit.

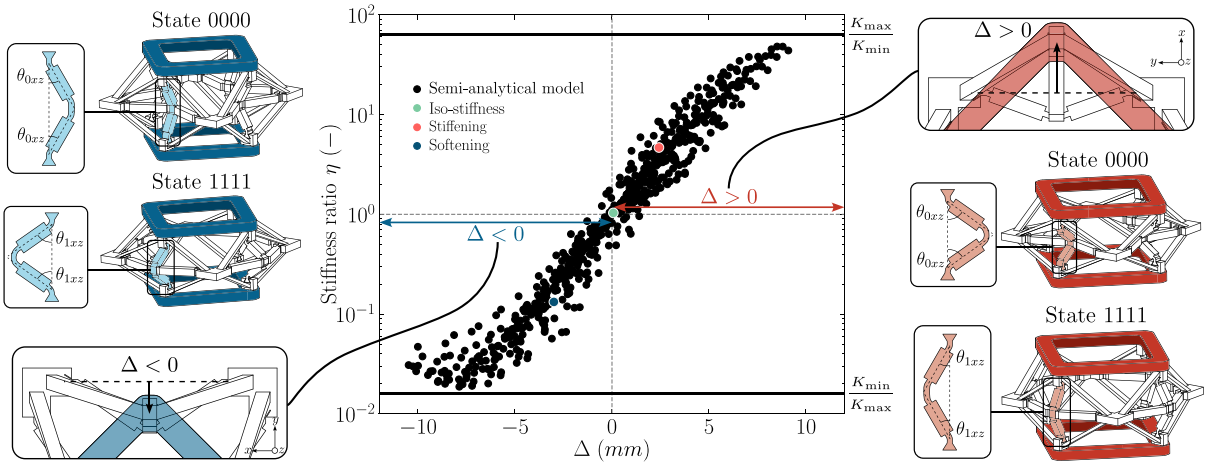

Figure 4. Evolution of the stiffness ratio as a function of Δ. The parameter Δ is defined as the algebraic distance between a first line connecting the two ends of von Mises truss in the *xz* plane and a second line connecting the ends of the von Mises truss in the *xy* plane. Through semi-analytical modeling, we show that when $\Delta = 0$, no change in stiffness is observed; however, when $\Delta < 0$, the stiffness decreases, and when $\Delta > 0$, the stiffness increases. The green, red, and blue points correspond to the iso-stiffness, stiffening, and softening units, respectively.

2.3. Post-Fabrication Modularity

Next, we now show that the reversible assembly process of the unit enables its stiffness variation, η, to be reprogrammed post-fabrication. For this, we start from the stiffening unit studied in Figure 3 with $r_L^{\text{stiff}} = 2.0$, $\theta_{0xy}^{\text{stiff}} = 20°$, $\theta_{0xz}^{\text{stiff}} = 55°$, and $L_{0xz}^{\text{stiff}} = 10$ mm (see **Figure 5**A(i)). The coupled von Mises trusses within each face of the unit can be substituted with a new geometry, forming a unit characterized by $r_L^{\text{stiff}'}$, $\theta_{0xy}^{\text{stiff}'}$, $\theta_{0xz}^{\text{stiff}'}$, provided that the new double von Mises truss is able to be attached to the original frame without deforming it (see Section S4, Supporting Information, for details on the geometric compatibility conditions). For example, we find that a double von mises truss characterized by $r_L^{\text{stiff}'} = 1.44$, $\theta_{0xy}^{\text{stiff}'} = 34°$, $\theta_{0xz}^{\text{stiff}'} = 67°$ with $L_{0xz}^{\text{stiff}'} = 16$ mm is compatible to the original stiffening unit. We 3D print this new unit with thermoplastic polyurethane (blue TPU 95 A from Polymaker with $E_0 = 28$ MPa—see Figure 7A(ii)). In Figure 5B, we report the force–displacement curves of the initial geometry (see the grey curves) and the new geometry (see the blue curves) under compression in both stable states. Whereas the original stiffening unit exhibits an experimental stiffness variation of $\eta_{\text{exp}}^{\text{stiff}} = 3.64$, the modified one with blue von Mises trusses displays an experimental stiffness variation of $\eta_{\text{exp}}^{\text{blue}} = 1.49$. While multistability alone enables in situ modification of the unit's effective stiffness in the two stable states, modularity increases tunability by allowing changes in the stiffness variation itself.

2.4. Sandwich Panel with Tunable Stiffness

We exploit the stiffness tunability of our mechanical metamaterial unit cell to build a sandwich panel displaying distinct compressive and bending stiffness. The panel is composed of six units enclosed between two acrylic plates (see **Figure 6**A). We select a unit exhibiting a significant height variation, which also proves to have a substantial change in stiffness. The process used to determine its geometry ($r_L^{\text{sandwich}} = 1.14$, $\theta_{0xy}^{\text{sandwich}} = 28°$, $\theta_{0xz}^{\text{sandwich}} = 58°$) is described in Section S4, Supporting Information. The unit is fabricated in six samples, which can be fixed in a reversible manner between two acrylic plates (see Figure 6A). First, we demonstrate in Figure 6B that the panel's compressive stiffness increases when all units are switched from state 0000 to state 1111. Indeed, as the stiffness in compression of a single unit increases when switching from state 0000 to state 1111 and since six units are combined in parallel, the effective experimental compressive stiffness of the panel increases as well, starting at $K_{0000}^{\text{sandwich}} = 45.4\ \text{N mm}^{-1}$ when all units are in state 0000 and rising to $K_{1111}^{\text{sandwich}} = 70.8\ \text{N mm}^{-1}$. The compressive stiffness measured experimentally for one unit is $K_{0000}^{\text{unit}} = 10.9\ \text{N mm}^{-1}$ in state 0000 and $K_{1111}^{\text{unit}} = 14.9\ \text{N mm}^{-1}$. As the six units are arranged in parallel, the expected stiffness of the panel are $6 \times K_{0000}^{\text{unit}} = 65.4\ \text{N mm}^{-1}$ in the first stable state and $6 \times K_{1111}^{\text{unit}} = 89.4\ \text{N mm}^{-1}$ in the second stable state. However, the experimentally measured values are significantly lower than these calculated predictions. This discrepancy is likely due to potential imperfections in the manufacturing of the units and the assembly of the panel. In addition to the compressive stiffness variation, two parallel phenomena lead to an increase in bending stiffness when switching from the first stable state to the second one. First, the core of the sandwich panel is stiffer when all the units are in state 1111 compared to state 0000. Second, as each unit's height increases by 18% upon actuation, the sandwich panel's overall thickness also increases, thereby redistributing the constituent material about the neutral axis and enhancing its second moment of area. By conducting a three-point bending test, we confirmed that the panel's bending stiffness increased from $5.28\ \text{N mm}^{-1}$ when all units are in state 0000 to $11.2\ \text{N mm}^{-1}$ when all units are in state 1111 (see Figure 6C).

2.5. Surface Morphing

Lastly, we fabricate a second sandwich panel consisting of an array of nine units, with an acrylic bottom surface and a top

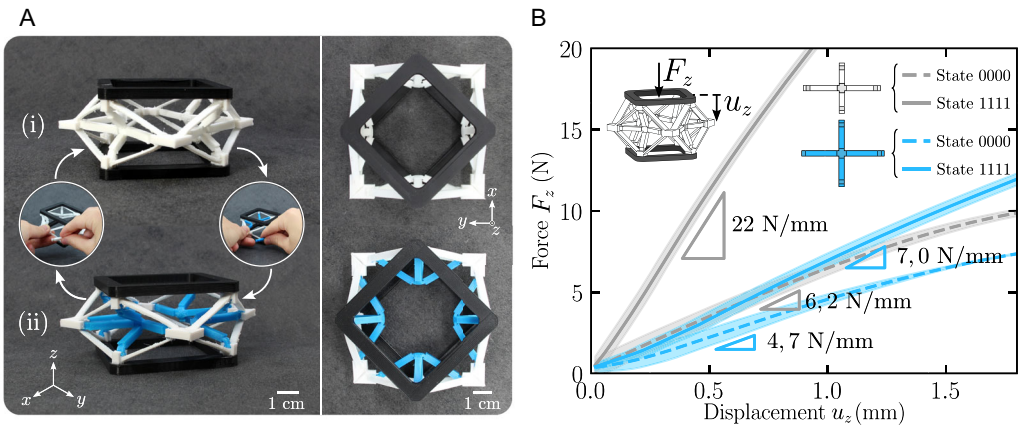

Figure 5. Post-fabrication reprogramming of stiffness variation through modularity. A) Using the reversibility of the assembly system described in Figure 3A(iii), we start from the stiffening unit pictured in i) $r_L = 2.0$, $\theta_{0xy} = 20°$, $\theta_{0xz} = 55°$ and obtain the unit shown in ii) $r_L = 1.44$, $\theta_{0xy} = 34°$, $\theta_{0xz} = 67°$ by replacing the coupled von Mises trusses within each face. B) This change in geometry results in a modification of the stiffness variation, as evidenced by the compression tests conducted. The experimental uncertainty is obtained by repeating the tests in compression five times.

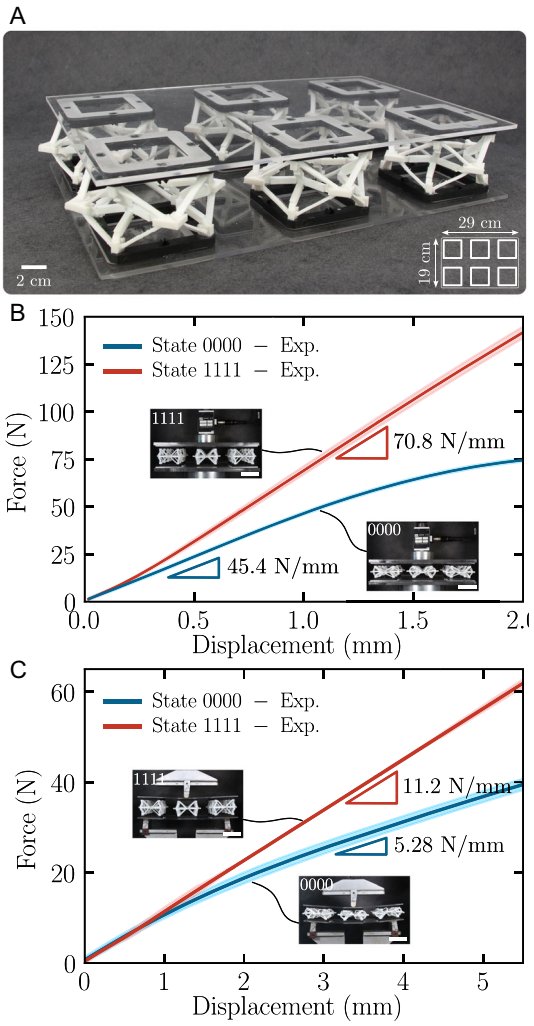

Figure 6. Application as a sandwich panel with tunable compressive and bending stiffness. A) The sandwich panel consists of an array of six units fixed between two acrylic plates. B) By performing a compression test, we demonstrate its capability to change compressive stiffness (scale bar is 5 cm). C) The three-point bending test reveals its ability to change bending stiffness (scale bar is 5 cm). The experimental uncertainty is obtained by repeating the tests in compression and bending five times.

surface made of a thin 3 mm layer of ethylene propylene diene monomer rubber to allow deformation. As the height of a unit can change when transitioning between stable states, actuating only one face allows the unit to bend about the axis perpendicular to its normal (see Figure 1F). To show that this enables control over the curvature of the top surface about the x and y axes, i.e., κ_x and κ_y, respectively, we consider two types of units with different geometries, denoted α and β. Importantly, these units are selected to maximize height variation while meeting two conditions. First, both units must be interchangeable, so that one can be replaced by the other to allow for adjustments in the achievable shapes of the panel. Second, to ensure continuity, unit β is chosen such that its height in state 0000 matches the height of unit α in state 1111. The process followed to select each unit geometry is detailed in Section S4, Supporting Information. In **Figure 7**, we highlight with green and blue squares the α and β units on schematics representing three different 3×3 arrangements of the sandwich panel. By selectively actuating different faces, we demonstrate that, depending on the geometry of the units, we can transition from a flat surface (Figure 7A) to

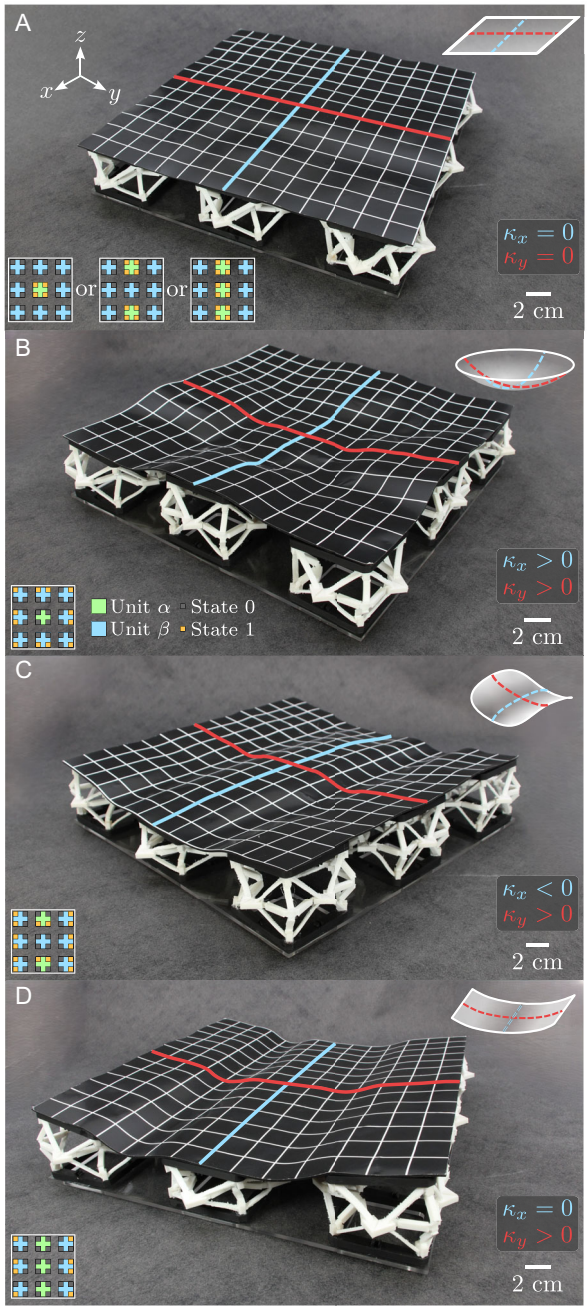

Figure 7. Application as a sandwich panel with morphing surfaces. A) Initially, the surface of the sandwich panel is flat. Two types of units with distinct geometries are utilized, designated as α and β. By selectively actuating the faces of the units, different shapes are obtained depending on the geometry of the units: B) a bowl, C) a saddle surface, and D) a cylindrical surface. A white grid has been added on the top surface to better visualize its 3D deformation.

different programmed shapes. First, by placing a unit α in the center and surrounding it with eight unit β, the height at the center of the panel can be reduced by switching unit α from the second stable state to the first. Simultaneously, the height at the edges can be increased by actuating the sides of the unit β in the corners of the panel, resulting in a bowl-shaped surface (Figure 7B). Next, we position two units α in the middle of two opposite sides of the panel. By deactivating the outward-facing sides of both unit α, we can induce a negative curvature along the x axis and, by activating the outward-facing sides of unit β, we can induce a positive curvature along the y axis, creating a saddle-shaped surface (Figure 7C). Finally, we place three units α in the center line along the x axis and six units β on the sides. By deactivating the faces of all unit α and by actuating the outward-facing sides of unit β, we create a zero curvature along the x axis and a positive curvature along the y axis, resulting in a cylindrical shape (Figure 7D). Although the top surface adapts well to the inclination of the unit cells, folds can appear when the curvature is positive. Negative curvature is also limited because the top surface is being stretched. These effects could be mitigated by using a softer material for the top surface and by increasing the number of units in the array to achieve a smoother surface.

3. Conclusions

In summary, we introduced a multistable mechanical metamaterial that leverages geometric frustration arising from the assembly of two coupled von Mises trusses to achieve in situ stiffness tunability, shape-morphing capabilities, and modularity. By modeling our unit cell both with FE methods and semi-analytical approaches, we identified various possible behaviors within distinct regions of our design space: 1) monostability, 2) no stiffness and height variation, 3) decreasing stiffness and height, and 4) increasing stiffness and height. Experimental validation was performed using 3D-printed prototypes, resulting in the development of several applications. These include demonstrating the post-fabrication reprogrammability of stiffness variation through the unit's modularity, creating a sandwich panel with tunable compressive and bending stiffness, and designing a sandwich panel capable of morphing a surface.

While this work primarily focused on the design and fabrication of the mechanical metamaterial, manual actuation is still required. Future work should explore remote actuation to enhance ease of use and broaden application potential, which can be achieved through the use of materials responsive to temperature,[15,41] magnetic fields,[16,17,42] and light,[43] using pneumatic actuation[44–47] or shape memory alloys.[48] Moreover, various multimaterial fabrication techniques[49] could be employed to improve the manufacturing process by reducing the number of parts to assemble and decreasing the scale of the unit cell, thereby expanding the range of potential applications. In this work, only the linear slope of the force–displacement curves generated by the FE and semi-analytical models was used to predict the stiffness of the unit in state 0000 and 1111. Predicting the entire curve through numerical simulations would be important in applications requiring large compression forces applied on the panels that could trigger buckling in the beams making the frame of the unit (see Figure S4, Supporting Information).

We believe that the major advance of the proposed concept lies in its combination of multiple functionalities, namely stiffness tunability, shape morphing, and modularity. The integration of these versatile attributes within a single unit showcases its potential to impact current mechanical metamaterial design, paving the way for innovative solutions in diverse engineering fields. Our concept could be applied in acoustics to build adaptive Helmholtz resonators by controlling the absorption frequencies based on shape[50] and stiffness,[51] in aerospace to passively contract and expand control surfaces to mitigate ice formation[52] or reduce drag,[53] and in biomedical engineering to build tunable prostheses and orthoses.[54] For all applications, the modularity of our mechanical metamaterials could be exploited to reprogram functionality.

4. Experimental Section

The design, materials, and fabrication methods are summarized in Section S1, Supporting Information. Details on the FE simulations are provided in Section S2, Supporting Information. The semi-analytical model is detailed in Section S3, Supporting Information. The process for selecting the different unit geometries for the applications is described in Section S4, Supporting Information.

Supporting Information

Supporting Information is available from the Wiley Online Library or from the author.

Acknowledgements

The authors acknowledge support from the Natural Sciences and Engineering Research Council of Canada.

Conflict of Interest

The authors declare no conflict of interest.

Author Contributions

Yannis Liétard: Conceptualization (supporting); Data curation (lead); Formal analysis (lead); Investigation (lead); Methodology (lead); Software (lead); Validation (lead); Visualization (lead); Writing—original draft (lead); Writing—review & editing (supporting). **Daniel Therriault**: Conceptualization (supporting); Formal analysis (supporting); Funding acquisition (equal); Investigation (equal); Methodology (equal); Project administration (equal); Resources (equal); Supervision (equal); Validation (supporting); Visualization (supporting); Writing—original draft (supporting); Writing—review & editing (equal). **David Melancon**: Conceptualization (lead); Formal analysis (supporting); Funding acquisition (equal); Investigation (equal); Methodology (equal); Project administration (equal); Resources (equal); Supervision (equal); Validation (supporting); Visualization (supporting); Writing—original draft (supporting); Writing—review & editing (equal).

Data Availability Statement

The data that support the findings of this study are available from the corresponding author upon reasonable request.

Keywords

additive manufacturings, mechanical metamaterials, multistabilities, tunable properties

Received: August 27, 2024
Revised: October 21, 2024
Published online: November 23, 2024

[1] A. A. Zadpoor, *Mater. Horiz.* **2016**, *3*, 371.
[2] K. Bertoldi, V. Vitelli, J. Christensen, M. Van Hecke, *Nat. Rev. Mater.* **2017**, *2*, 17066.
[3] P. Jiao, J. Mueller, J. R. Raney, X. Zheng, A. H. Alavi, *Nat. Commun.* **2023**, *14*, 6004.
[4] J. T. B. Overvelde, T. A. De Jong, Y. Shevchenko, S. A. Becerra, G. M. Whitesides, J. C. Weaver, C. Hoberman, K. Bertoldi, *Nat. Commun.* **2016**, *7*, 10929.
[5] Z. Zhai, Y. Wang, K. Lin, L. Wu, H. Jiang, *Sci. Adv.* **2020**, *6*, eabe2000.
[6] X. Wang, H. Qu, X. Li, Y. Kuang, H. Wang, S. Guo, P. Sharma, *PNAS Nexus* **2023**, *2*, pgad098.
[7] Y. Yang, M. A. Dias, D. P. Holmes, *Phys. Rev. Mater.* **2018**, *2*, 110601.
[8] Z. Zhai, Y. Wang, H. Jiang, *Proc. Natl. Acad. Sci.* **2018**, *115*, 2032.
[9] H. Fang, S.-C. A. Chu, Y. Xia, K.-W. Wang, *Adv. Mater.* **2018**, *30*, 1706311.
[10] Z. Wo, E. T. Filipov, *Extreme Mech. Lett.* **2023**, *58*, 101941.
[11] Q. Liu, H. Ye, J. Cheng, H. Li, X. He, B. Jian, Q. Ge, *Acta Mech. Solida Sin.* **2023**, *36*, 582.
[12] J. L. Silverberg, A. A. Evans, L. Mcleod, R. C. Hayward, T. Hull, C. D. Santangelo, I. Cohen, *Science* **2014**, *345*, 647.
[13] L. Wu, D. Pasini, *Phys. Rev. Appl.* **2023**, *19*, L061001.
[14] L. Wu, D. Pasini, *Nat. Commun.* **2024**, *15*, 3087.
[15] J. Mueller, J. A. Lewis, K. Bertoldi, *Adv. Funct. Mater.* **2022**, *32*, 2105128.
[16] J. A. Jackson, M. C. Messner, N. A. Dudukovic, W. L. Smith, L. Bekker, B. Moran, A. M. Golobic, A. J. Pascall, E. B. Duoss, K. J. Loh, C. M. Spadaccini, *Sci. Adv.* **2018**, *4*, eaau6419.
[17] T. Chen, M. Pauly, P. M. Reis, *Nature* **2021**, *589*, 386.
[18] Y. Tang, Y. Chi, J. Sun, T.-H. Huang, O. H. Maghsoudi, A. Spence, J. Zhao, H. Su, J. Yin, *Sci. Adv.* **2020**, *6*, eaaz6912.
[19] Y. Wang, L. Li, D. Hofmann, J. E. Andrade, C. Daraio, *Nature* **2021**, *596*, 238.
[20] S. Mintchev, J. Shintake, D. Floreano, *Sci. Rob.* **2018**, *3*, eaau0275.
[21] G. Librandi, E. Tubaldi, K. Bertoldi, *Nat. Commun.* **2021**, *12*, 3454.
[22] H. Mofatteh, B. Shahryari, A. Mirabolghasemi, A. Seyedkanani, R. Shirzadkhani, G. Desharnais, A. Akbarzadeh, *Adv. Sci.* **2022**, *9*, 2202883.
[23] Q. Zhong, J. Zhu, F. E. Fish, S. J. Kerr, A. M. Downs, H. Bart-Smith, D. B. Quinn, *Sci. Rob.* **2021**, *6*, eabe4088.
[24] C. Coulais, E. Teomy, K. De Reus, Y. Shokef, M. Van Hecke, *Nature* **2016**, *535*, 529.
[25] D. Raviv, W. Zhao, C. Mcknelly, A. Papadopoulou, A. Kadambi, B. Shi, S. Hirsch, D. Dikovsky, M. Zyracki, C. Olguin, R. Raskar, S. Tibbits, *Sci. Rep.* **2014**, *4*, 7422.
[26] R. Guseinov, C. Mcmahan, J. Pérez, C. Daraio, B. Bickel, *Nat. Commun.* **2020**, *11*, 237.
[27] D. Hwang, E. J. Barron, A. B. M. T. Haque, M. D. Bartlett, *Sci. Rob.* **2022**, *7*, eabg2171.
[28] T. Chen, K. Shea, *Mater. Des.* **2021**, *205*, 109688.
[29] Y. Zhang, M. Tichem, F. Van Keulen, *Extreme Mech. Lett.* **2022**, *51*, 101553.
[30] B. Haghpanah, L. Salari-Sharif, P. Pourrajab, J. Hopkins, L. Valdevit, *Adv. Mater.* **2016**, *28*, 7915.
[31] A. S. Meeussen, M. Van Hecke, *Nature* **2023**, *621*, 516.
[32] P. H. De Jong, Y. Salvatori, F. Libonati, M. J. Mirzaali, A. A. Zadpoor, *Mater. Des.* **2023**, *235*, 112427.
[33] G. Risso, M. Kudisch, P. Ermanni, C. Daraio, *Adv. Sci.* **2024**, *11*, 2308903.
[34] D. Terwagne, M. Brojan, P. M. Reis, *Adv. Mater.* **2014**, *26*, 6608.
[35] F. S. L. Bobbert, S. Janbaz, T. Van Manen, Y. Li, A. A. Zadpoor, *Mater. Des.* **2020**, *191*, 108624.
[36] Y. Li, Q. Zhang, Y. Hong, J. Yin, *Adv. Funct. Mater.* **2021**, *31*, 2105641.
[37] J.-J. Mao, S. Wang, W. Tan, M. Liu, *Eng. Struct.* **2022**, *272*, 114976.
[38] Y. Li, A. Di Lallo, J. Zhu, Y. Chi, H. Su, J. Yin, *Nat. Commun.* **2024**, *15*, 6247.
[39] Y. Zhu, E. T. Filipov, *Nat. Commun.* **2024**, *15*, 2353.
[40] Y. Chi, Y. Li, Y. Zhao, Y. Hong, Y. Tang, J. Yin, *Adv. Mater.* **2022**, *34*, 2110384.
[41] H. Niknam, A. Akbarzadeh, D. Therriault, S. Bodkhe, *Appl. Mater. Today* **2022**, *28*, 101529.
[42] V. Ramachandran, M. D. Bartlett, J. Wissman, C. Majidi, *Extreme Mech. Lett.* **2016**, *9*, 282.
[43] M. R. Shankar, M. L. Smith, V. P. Tondiglia, K. M. Lee, M. E. Mcconney, D. H. Wang, L.-S. Tan, T. J. White, *Proc. Natl. Acad. Sci.* **2013**, *110*, 18792.
[44] D. Melancon, B. Gorissen, C. J. García-Mora, C. Hoberman, K. Bertoldi, *Nature* **2021**, *592*, 545.
[45] D. Melancon, A. E. Forte, L. M. Kamp, B. Gorissen, K. Bertoldi, *Adv. Funct. Mater.* **2022**, *32*, 2201891.
[46] B. Gorissen, D. Melancon, N. Vasios, M. Torbati, K. Bertoldi, *Sci. Rob.* **2020**, *5*, eabb1967.
[47] S. Rahman, L. Wu, A. El Elmi, D. Pasini, *Adv. Funct. Mater.* **2023**, *33*, 2304151.
[48] S. Barbarino, F. S. Gandhi, R. Visdeloup, in *A Bi-stable Von-Mises Truss for Morphing Applications Actuated Using Shape Memory Alloys in Volume 1: Development and Characterization of Multifunctional Materials; Modeling, Simulation and Control of Adaptive Systems; Integrated System Design and Implementation*, American Society of Mechanical Engineers, Snowbird, USA, **2013**, p. V001T01A004.
[49] X. Zhou, L. Ren, Z. Song, G. Li, J. Zhang, B. Li, Q. Wu, W. Li, L. Ren, Q. Liu, *Composites, Part B* **2023**, *254*, 110585.
[50] G. Wen, S. Zhang, H. Wang, Z.-P. Wang, J. He, Z. Chen, J. Liu, Y. M. Xie, *Int. J. Mech. Sci.* **2023**, *239*, 107872.
[51] Y. Aurégan, *Appl. Phys. Lett.* **2018**, *113*, 201904.
[52] O. Tamer, A. Kyriazis, M. Sinapius, *Smart Mater. Struct.* **2020**, *29*, 045021.
[53] T. Mkhoyan, N. R. Thakrar, R. De Breuker, J. Sodja, in *AIAA Scitech 2021 Forum*, American Institute of Aeronautics and Astronautics, VIRTUAL EVENT **2021**.
[54] M. J. Mirzaali, A. A. Zadpoor, *APL Bioeng.* **2024**, *8*, 010901.